sustainability

MDPI

Article

Adsorption of Phosphate from Aqueous Solution Using Hydrochar Produced from Agricultural Wastes

Esha Shrestha, Ashish Manandhar and Ajay Shah *

Department of Food, Agricultural and Biological Engineering, The Ohio State University, Wooster, OH 44691, USA; shrestha.64@buckeyemail.osu.edu (E.S.); manandhar.5@osu.edu (A.M.)
* Correspondence: shah.971@osu.edu

Abstract: Excess phosphorus (P) in agricultural runoff can cause eutrophication in nearby waterbodies. Therefore, it is crucial to remove P from agricultural runoff before it reaches aquatic environments. This study evaluated the P adsorption potential of adsorbents prepared via co-hydrothermal carbonization of multiple agricultural wastes, including dairy manure (DM), corn stover (CS), and eggshell (ES), followed by thermal activation. The performance of the prepared adsorbents was investigated by both batch and column experiments. The activated hydrochar (AHC) with a DM/CS/ES ratio of 1:0:1 showed the highest P adsorption capacity of 209 ± 0.6 and 65.97 ± 9.04 mg/g in batch and column experiments, respectively. The P adsorption mechanism was well described by the Langmuir isotherm model (R^2 > 0.8802) and the pseudo-second-order kinetics model (R^2 > 0.8989). The adsorbent indicated the longest breakthrough and exhaust time of 210 and 540 min, respectively, with an adsorbent dose of 1 g and an initial concentration of 25 mg P/L. The breakthrough curve was well described by the Thomas model (R^2 > 0.971). Thus, this study indicates that AHC with eggshell has high potential for use as an adsorbent for P removal from agricultural runoff.

Keywords: phosphorus; agricultural waste; eggshell; eutrophication; hydrothermal carbonization; hydrochar; waste valorization

Citation: Shrestha, E.; Manandhar, A.; Shah, A. Adsorption of Phosphate from Aqueous Solution Using Hydrochar Produced from Agricultural Wastes. *Sustainability* **2024**, *16*, 9259. https://doi.org/10.3390/su16219259

Academic Editors: Carin Sjöstedt, Sara Silva, Alessandra Braga Ribeiro, Yuxue Liu, Carlos Miguel Henriques Ferreira and Catarina Silva S. Oliveira

Received: 8 August 2024
Revised: 8 September 2024
Accepted: 22 October 2024
Published: 25 October 2024

1. Introduction

In the last century, man-made fertilizers have greatly increased crop productivity, allowing farmers to grow more crops on less land [1]. Agriculture in the U.S. relies heavily on fertilizers to meet the nutrient requirements of crops, with nitrogen (N), phosphorus (P), and potassium (K) being the primary nutrients of focus [2]. While fertilizers contribute significantly to agricultural productivity, their excessive or improper use can lead to environmental degradation, including water pollution and soil erosion. Agricultural runoff is one of the main sources of nutrient pollution, mainly P, in waterbodies [3], and around 80% of globally mined P is used in agriculture [4]. Out of the 24 million metric tons of P used in agriculture annually, around 4 million tons (Mt) of P is lost via surface runoff [5]. The inflow of P in different lakes around the world between the periods 1990–1994 and 2005–2010 has increased by 82%, 38%, and 17% in Latin America, North America, and Africa, respectively [6]. This excess P discharge into waterbodies provides nutrients that enable algae to grow rapidly, leading to harmful algal blooms (HABs). HABs have led to major environmental and human health problems in most parts of the U.S., including the Great Lakes, Chesapeake Bay, and Gulf of Mexico [4,7–10]. In Lake Erie, HABs have cost millions of dollars due to decreasing tourism, recreation, and fishing-related revenues and reduced property values [11]. It is therefore important to remove or control excess P from agricultural runoff prior to its discharge into natural waterbodies. In addition, P reserve in nature is limited, and as its demand continues to increase, its reserve will be exhausted [12,13]. Hence, more research needs to focus on the development of technologies to trap excess P from runoff to reduce eutrophication and solve the global scarcity of P. The problem can be addressed by recycling excess P in water [13].

Traditional methods for P removal, such as chemical precipitation and biological treatment, often come with drawbacks such as high cost, limited efficiency, and the generation of chemical sludge, which is generally disposed of in a landfill [12,14]. The adsorption process is easy to operate and efficient for the removal of pollutants from water [13,15]. Activated carbon produced from non-renewable sources, including coal and petroleum, has been widely used as adsorbents in water treatment due to its large surface area and chemical stability [16,17]. Recently, utilization of low-cost sustainable materials, including agricultural and industrial wastes such as peanut shell [18], rice straw [13,19], corn stover [15,20,21], rape straw [22], coconut shell [23], wheat straw [24,25], alkaline residue by-product from soda ash production [26], dyeing sludge [27], sewage sludge [23,28,29], etc., has been widely investigated to produce biochar via pyrolysis for P removal.

Pyrolysis is a thermochemical conversion technology that operates in an inert environment at temperatures above 400 °C and is suitable for dry feedstock [30]. Wet feedstocks such as dairy manure have a high moisture content (>80%) and require high energy for drying [30,31]. Animal manure is widely produced in the U.S. and is being increasingly concentrated in large animal farms, with 1.3 billion metric tons of animal manure being generated annually in the U.S. [32]. Dairy manure, if not managed properly, can lead to nutrient losses and greenhouse gas emissions [30]. Hydrothermal carbonization (HTC) operates at 180 to 300 °C under subcritical water conditions and is suitable to treat wet feedstocks with 75–90% moisture content, as the water contained in the raw feedstock can be directly used as reaction medium [30,33]. Co-hydrothermal carbonization (Co-HTC) of low-moisture feedstock, such as corn stover, with dairy manure can decrease the water requirement of the HTC process for dry feedstock while increasing the surface area of the hydrochar [34], which can improve its adsorption performance. Corn stover is the most abundant agricultural residue in the U.S., with 109 million metric tons (dry) of corn stover available every year [35]. About 190 to 290 million metric tons (dry) of crop residues could be available by 2030, with corn stover comprising approximately 85% of this total quantity [36].

Hydrochar and biochar have strong affinity towards cations and organic pollutants such as dyes, pesticides, and pharmaceuticals but show weak adsorption for anionic pollutants such as P [13]. For example, biochar prepared from cow manure showed maximum adsorption of 175.53 and 68.08 mg/g for Pb^{2+} and Cd^{2+}, respectively [37]. Similarly, high adsorption of methylene blue (258.97 mg/g) was reported for hydrochar prepared by Co-HTC of polyvinyl chloride and bamboo [38]. Modification of char with metal cations such as Fe^{3+}, Ca^{2+}, Mg^{2+}, Al^{3+}, etc. has been shown to improve the P adsorption capacity [13,20,29,33,39,40]. Shin et al. (2020) [41] used Mg-modified biochar produced from ground coffee waste to remove P and found that the control, i.e., the unmodified biochar, did not adsorb P, whereas maximum P adsorption of 56 mg P/g was reported for the modified biochar. Another study evaluated Mg-modified biochar derived from sugarcane residue and obtained maximum P adsorption of 121.25 mg/g [42]. Wang et al. (2018) [43] reported a maximum adsorption capacity of 314.22 mg P/g for biochar prepared from calcium hydroxide ($Ca(OH)_2$) and flour in a mass ratio of 2:1. Similarly, Kong et al. (2018) [27] mixed calcium carbonate ($CaCO_3$) and sludge in the ratio of 1:2 and obtained a maximum adsorption capacity of 116.82 mg P/g. Eggshell is a biowaste that is composed of >95% $CaCO_3$ and can be used to replace a chemical source of calcium for the activation of hydrochar [13,20]. According to the U.S. Department of Agriculture, 91 billion eggs were produced in 2006, generating 455,000 tons of waste eggshell. A previous study reported improved P adsorption from 5.21 to 231 mg/g after modification of biochar prepared from rice straw with eggshell [13]. Similarly, Cao et al. (2020) [22] compared the P adsorption performance of modified biochar prepared from rapeseed using chemical $CaCO_3$ and eggshell as a source of calcium and found better adsorption of eggshell-modified biochar (104.7 mg P/g) compared to $CaCO_3$-modified biochar (96.7 mg P/g).

Previous studies have investigated the properties of hydrochar produced from a wide range of feedstocks for use as soil amendment [28,44] and biofuel [21,30] and for the adsorption of organic pollutants [38,45,46]. However, research investigating mixed feedstock such as animal manure, agricultural residues, and eggshell and processing approaches such as HTC and thermal activation to produce suitable P adsorbents is still lacking. The main objective of this study was to assess the effectiveness of an adsorbent derived from co-hydrothermal carbonization of dairy manure, corn stover, and eggshell, followed by thermal activation, for P adsorption. This was achieved by investigating the impact of hydrothermal carbonization and thermal activation on P adsorption through batch experiments and continuous fixed-bed column experiments. The promising adsorbents identified in this study can be used in nutrient removal structures to adsorb P from agricultural runoff, hence reducing nutrient loads in nearby water bodies. This approach not only provides a sustainable approach for phosphate removal but also addresses waste management issues related to both wet and dry agricultural wastes. Additionally, using P-rich hydrochar after adsorption as a source of fertilizer can replace the requirement for mined P fertilizer, hence promoting a circular economy by closing the P loop.

2. Materials and Methods

2.1. Experimental Design and Statistical Analysis

Batch and column studies were conducted to investigate the hypothesis that the addition of eggshell and corn stover to dairy manure can enhance its P adsorption potential. Two independent variables were considered for this study: (1) feedstock mixes and (2) processing methods. The feedstock mixes considered for this experiment consisted of a control, i.e., dairy manure-derived adsorbent, and six treatments with varying ratios of dairy manure, corn stover, and eggshell (Table 1). The processing methods included HTC only (without activation) and thermal activation of feedstock mixes with and without HTC. The response variable was the P adsorption capacity, which was quantified to determine the effectiveness of each treatment. By analyzing the P adsorption data, the study aimed to identify the optimal mix ratio and processing method that maximizes the P adsorption potential of a dairy manure-based adsorbent.

Table 1. Mix ratios of dairy manure (DM), corn stover (CS), and eggshell (ES) for adsorbent preparation.

Treatments	Feedstock Mix DM/CS/ES	Justification for Selection
1	1:0:0	Control dairy manure (DM)
2	1:1:0	Test impact of corn stover (CS)
3	2:1:0	Test if similar results can be obtained with less quantity of CS
4	1:0:1	Test impact of eggshell (ES)
5	2:0:1	Test if similar results can be obtained with less quantity of ES
6	1:1:1	Test combined effect of CS and ES
7	2:1:1	Test combined effect with less CS and ES

Four feedstock mixes with different ratios of dairy manure, corn stover, and eggshell were selected for column adsorption, and a full factorial design was performed (Table S1) to explore the effect of adsorbent dose and initial concentration on P adsorption in a fixed-bed column. Adsorbent doses of 0.5 and 1 g and initial concentrations of 25 and 50 mg/L were used. The flow rate was fixed at 5 mL/min. A total of 48 column runs were performed in this study.

All the analyses were performed in triplicate. Statistical analysis was performed using Microsoft Excel (Version 2408), while SAS Studio was employed for ANOVA and least squares difference (LSD) means comparison at p-value < 0.05. Graphs and model fitting were carried out using the OriginPro software (Version 2024), and the coefficient of determination (R^2) obtained was used to compare the applicability of the model.

2.2. Materials

Dairy manure was collected from the dairy farm located at the Ohio State University, Wooster Campus, OH, and was stored in a plastic container at 4 °C in a cold store. Corn stover was collected from the research plot in Wooster Campus, OH. The collected corn stover was milled using a knife mill with a 1 mm particle size mesh (Thomas Wiley Mill Model 4, Thomas Scientific, Swedesboro, NJ, USA). Eggshell was collected from kitchen waste, washed with distilled water to remove any impurities, and ground using a ball mill. The milled eggshell was passed through a sieve with a 0.8 mm mesh size. For all the individual feedstocks, the moisture content was determined using the oven dry method [47], and the ash content was determined using a muffle furnace (Model FO100CR, Yamato Scientific America, Inc, Santa Clara, CA, USA) [48] (Table S2). Moisture content and ash content of different feedstock mixes were estimated based on the experimental values for the individual feedstocks and their mix ratios. Potassium dihydrogen phosphate (KH_2PO_4), sulfuric acid, ascorbic acid, potassium antimony tartrate, ammonium molybdate, glass beads, and glass wool required for the adsorption experiment were purchased from Sigma Aldrich (St. Louis, MO, USA).

2.3. Preparation of Adsorbents

2.3.1. Hydrochar Production

Dairy manure, corn stover, and eggshell were mixed in different ratios to prepare 7 feedstock mixes. The total solid content of all the mixes was adjusted to 15%. For each HTC run, a total volume of 400 mL sample was loaded in a 1 L stirred-pressure Parr reactor (Model no. PARR 4843 1L, Parr Instrument Company, Moline, IL, USA). The samples were hydrothermally carbonized at 220 °C for 1 h. The reactor was then cooled down to room temperature, and the slurry was filtered using Whatman No. 1 filter paper. The solid, also known as filter cake, was dried at 50 °C to produce hydrochar, which was stored in an airtight container with a proper label. The experiment was performed in triplicate, and a total of 21 HTC runs were carried out in this study.

2.3.2. Activation

Hydrochar produced via HTC of the feedstock mixes and the feedstock mixes without HTC were placed in a crucible with lid and heated in a muffle furnace (Model FO100CR, Yamato Scientific America, Inc, Santa Clara, CA, USA) in the presence of N_2 at a flow rate of 3 L/min (Figure 1). The temperature was first held at 100 °C for 10 min to create an inert N_2 environment inside the furnace to limit the combustion due to the presence of O_2. The temperature was then increased to 800 °C at the rate of 40 °C/min and held at that temperature for 2 h. The activation temperature of 800 °C was chosen to facilitate complete calcination of $CaCO_3$ in the eggshell [49,50]. The adsorbents, i.e., hydrochar (HC), activated hydrochar (AHC), and the activated feedstock mixes without HTC (AFM), were stored in an airtight container until further use.

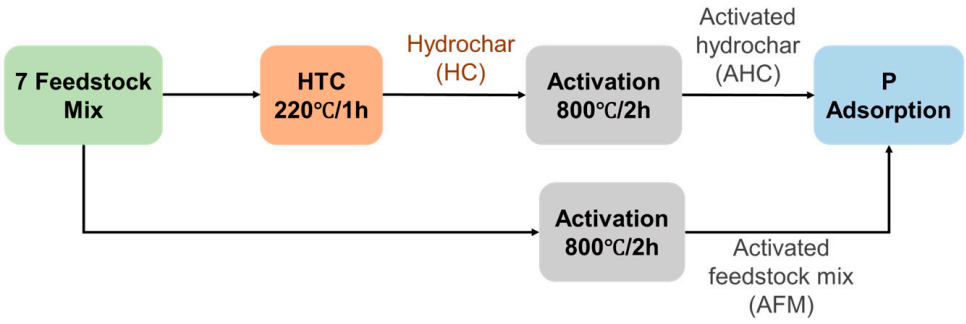

Figure 1. Schematic representation of the adsorbent preparation.

2.4. Characterization of Feedstocks and Adsorbents

The adsorbents before and after P adsorption were characterized using scanning electron microscopy (SEM-SU5000 FE-SEM, Schaumburg, IL, USA) for surface morphology. A Fourier transform infrared spectrometer (FTIR-Perkin-Elmer Spectrum Two, Shelton, CT, USA) within the spectral region of 4000 to 400 cm^{-1} was used to determine different functional groups on the adsorbent surface. The abovementioned samples, along with their raw feedstocks (dairy manure, corn stover, and eggshell), were also analyzed for Ca and P contents using inductively coupled plasma optical emission spectroscopy (Agilent 5110 ICP-OES, Agilent Technologies, Santa Clara, CA, USA), and carbon (C) and nitrogen (N) were determined using an elementar analyzer (CN628, LECO Corporation, St. Joseph, MI, USA).

2.5. Phosphate Adsorption in Batch Experiment

Batch adsorption experiments were carried out in triplicates to investigate the P adsorption capacity of adsorbents. The colorimetric method developed by the U.S. Environmental Protection Agency (EPA) [51] was followed to prepare the stock P solution and determine the P concentrations before and after adsorption. A phosphate stock solution of 5000 mg/L was prepared by dissolving KH_2PO_4 in deionized water, which was diluted to the required concentration as needed [51]. In a flask, 0.05 g of adsorbents (HC, AHC, and AFM) were added to 50 mL of a P solution of 400 mg/L concentration [22,33]. The adsorbent dose and initial P concentration were selected to ensure complete utilization of the adsorbents to determine their maximum P adsorption capacity. The flasks were transferred to a shaker incubator (New Brunswick Innova 43, Fischer Scientific, Waltham, MA, USA) and oscillated at 25 °C/150 rpm for 24 h. The solution was then filtered using a 0.45 µm syringe filter, and the final concentration of P in the filtrate was measured at the wavelength of 880 nm by the colorimetric method [51] using a UV spectrophotometer (BioMate 3S Spectrophotometer, Thermo Scientific, Waltham, MA, USA).

The amount of P adsorbed per unit mass of adsorbent was estimated using Equation (1):

$$q_e = (C_o - C_e)V/m \quad (1)$$

where q_e is the amount of P adsorbed per unit mass of adsorbent in mg/g, C_0 and C_e are the initial and equilibrium concentrations in mg/L, V is the volume of solution in L, and m is the mass of adsorbent in g.

The AHC performed better in batch experiments; hence, the adsorption behavior of AHC was further investigated in adsorption isotherm and kinetic experiments. The adsorption isotherm experiment was performed by adding 0.05 g of adsorbent in 50 mL of P solution of various concentrations (25, 50, 100, 200, 300, 400, and 500 mg/L), and their impact on the amount of P adsorbed per unit mass of adsorbent was evaluated [22,33]. Two widely used isotherm models, Langmuir and Freundlich, were used to fit the experimental data to examine the P adsorption behavior. The non-linear forms of Langmuir and Freundlich equations are given below [18,22,52]:

Langmuir equation:

$$q_e = \frac{q_m K_L C_e}{1 + K_L C_e} \quad (2)$$

where C_e (mg/L) is the concentration of the adsorbate at equilibrium, K_L (L/mg) is the Langmuir constant, q_e (mg/g) is the amount of P adsorbed at equilibrium, and q_m (mg/g) is the maximum adsorption capacity estimated by the model.

Freundlich equation:

$$q_e = K_F {C_e}^{1/n} \quad (3)$$

where C_e (mg/L) is the concentration of adsorbate at equilibrium; K_F ($mg^{(1-1/n)}\ L^{1/n}/g$) is the Freundlich constant; n is the heterogeneity constant, i.e., the greater the value of n, the higher the heterogeneity of the surface; and q_e is the amount of P adsorbed at equilibrium (mg/g).

The adsorption kinetics experiment was performed to determine the performance of the adsorbent over time. For this, 0.01 g of adsorbent was mixed in 50 mL of 100 mg/L P solution [13,18,20]. A 2 mL aliquot was filtered at predetermined time intervals (5, 15, 30, 60, 120, 240, 360, 720, and 1440 min), as suggested in previous studies [13,33]. Pseudo-first-order and pseudo-second-order kinetics models were used to fit the experimental data to investigate the mechanism of P adsorption on the AHC. The non-linear forms of pseudo-first-order and pseudo-second-order equations are given below:

Pseudo-first-order equation:

$$q_t = q_e(1 - e^{k1t}) \quad (4)$$

Pseudo-second-order equation:

$$q_t = \frac{q_e^2\, k_2\, t}{1 + q_e k_2 t} \quad (5)$$

where q_t (mg/g) is the amount adsorbed at time t, q_e is the amount adsorbed at equilibrium (mg/g), k_1 and k_2 are the first- and second-order rate constants, and t (min) is the time interval at which the samples were collected. k_1 is determined from the slope, q_e is determined from the intercept of the ln (q_e–q_t) versus t plot, and k_2 and q_e are calculated from the plot of t/q_t versus t.

2.6. Phosphate Adsorption in Fixed-Bed Column Experiment

A transparent polyvinyl chloride (PVC) column (20 cm in length and 1.9 cm in diameter) was packed in order with glass beads and glass wool, and 0.5–1 g of adsorbent was filled in the middle of the column and topped with a layer of glass wool and glass beads to keep the adsorbent in place during the adsorption experiment (Figure S1). The P solution of known concentrations (25 and 50 mg/L) was pumped through the column at a flow rate of 5 mL/min using a peristaltic pump (3385 variable-speed peristaltic tubing pump, Traceable, Webster, TX, USA). The effluent, after passing through the adsorption bed, was collected from the top of the column every 15 min and analyzed for P concentration. The collected samples were filtered with a 0.45 µm polyethersulfone (PES) syringe, and the P concentration was determined by the colorimetric method [51], where P reacted with molybdate in an acid medium to produce a blue-colored complex. The intensity of the blue color was proportional to the P concentration. The absorbance was measured at 880 nm using a UV spectrophotometer (BioMate 3S Spectrophotometer, Thermo Scientific, Waltham, MA, USA). As the adsorbent bed gradually saturated, the concentration in the effluent started to rise. The operation was stopped when the effluent P concentration was approximately equal to the influent P concentration, and the performance of the column was studied using a breakthrough curve (Figure S2).

Thomas Model

The relationship between concentration and time provides insight into the adsorbent's affinity for the adsorbate [53]. Additionally, predicting the concentration profile over time of the breakthrough curve is crucial for effectively designing an adsorption column [53,54]. Several adsorption models, such as the Adams–Bohart model [53,55,56], the Yoon–Nelson model [53,55,57], and the Thomas model [53,56,58], have been used to predict the dynamic adsorption behavior of adsorbents in fixed beds for various pollutants, including P. The Thomas model is one of the most widely used theoretical model to predict column performance [26,58,59] and is also suitable for determining the maximum adsorption capacity [53,60]. The Thomas model assumes a constant adsorption rate during the adsorption process and is limited by mass transfer at the interface, which can sometimes lead to inaccurate predictions. The non-linear Thomas model can be described by the following equation:

$$\frac{C_t}{C_0} = \frac{1}{1 + \exp\left(k_{th} * q_0 * \frac{m}{Q} - k_{th} * C_0 * t\right)} \quad (6)$$

where C_t (mg/L) is the effluent concentration, C_0 (mg/L) is the influent concentration, k_{th} (mL/min.mg) is the Thomas rate constant, q_0 (mg/g) is the predicted adsorption capacity, m (g) is the mass of the adsorbent packed in the column, and Q (mL/min) is the flow rate. The parameters k_{th} and q_0 are determined by fitting the experimental breakthrough curve data to the Thomas model equation.

3. Results and Discussion

3.1. HTC and Activation Yields

The average hydrochar yields for different feedstock mixes (DM/CS/ES) ranged from 58% to 68% (of dry feedstock) (Table 2). Decreases in hydrochar yields were observed when corn stover was mixed with dairy manure in ratios of 1:1 and 1:2. Previous research on HTC of mixed feedstocks indicated the presence of no synergism as well as both positive and negative synergism in terms of hydrochar yield [21,34,61]. Mariuzza (2022) [34] found a 1% to 5% decrease in hydrochar yield for a mixture of dairy manure and corn stover and a 2% to 6% decrease for a mixture of dairy manure and grape marc. However, a higher hydrochar yield between 1% and 13% was reported for a mixture of sewage sludge and banana stalk [61].

Table 2. HTC and activation yields for different feedstock mixes.

Feedstock Mix DM/CS/ES	HTC Yield (% of Dry Feedstock)	Activation Yield (% of Dry Hydrochar)
1:0:0	67.7 ± 1.86^{a}	27.0 ± 1.32^{B}
1:1:0	59.7 ± 0.323^{b}	28.4 ± 1.26^{B}
2:1:0	58.4 ± 0.747^{b}	27.3 ± 0.46^{B}
1:0:1	66.1 ± 0.902^{a}	47.9 ± 4.39^{A}
2:0:1	63.9 ± 0.72^{ab}	35.9 ± 2.77^{B}
1:1:1	67 ± 0.872^{a}	35.4 ± 1.43^{B}
2:1:1	65.7 ± 1.36^{a}	34.8 ± 1.83^{B}

Note: Values are means ± standard error of means. Treatments with different superscript letters within a column are statistically different ($p < 0.05$) as analyzed by one-way ANOVA and the LSD test.

The average AHC yields for different mixes ranged from 23% to 48% (of dry hydrochar). The decrease in yield after activation was probably due to the loss of volatile matter and destruction of cellulose, hemicellulose, and lignin in the feedstock at high temperatures [62–64]. Previous studies have reported a large decrease in yield between 100 and 350 °C due to the destruction of cellulose and hemicellulose, and a further decrease in yield was observed at temperatures >350 °C due to the linear loss of lignin mass with increasing temperature [62,63]. An increase in AHC yield was observed with the increase in eggshell in the mix. The highest yield was observed for the mix with the highest mass ratio of eggshell, i.e., DM/CS/ES ratio of 1:0:1, which can be explained by the higher ash content in eggshell ~94% (Table S1).

3.2. Characterization of Feedstocks and Adsorbents

The major elements of the prepared adsorbents (HC, AHC, and AFM) along with their raw feedstocks are shown in Table 3. An increase in C, N, Ca, and P content was observed after HTC and activation for feedstock mixes without eggshell. The increase in C, N, Ca, and P as compared to their respective feedstocks could be due to the degradation of organic matter and increase in concentration of minerals during activation at higher temperatures [62–64]. An overall increase in C content could be due to the lowering of H and O contents in the feedstock at higher temperatures as a result of the degradation of carbohydrate [62,63]. However, the lower carbohydrate content and higher protein and

lipid content in DM could have resulted in less carbonization in AHC produced with a DM/CS/ES ratio of 1:0:0 [65].

Table 3. Major elements of hydrochar (HC) before and after activation (AHC) and P adsorption (P-AHC).

Feedstock Mix DM/CS/ES	C (%)			N (%)			Ca (%)			P (%)			
	Raw	HC	AHC	Raw	HC	AHC	Raw	HC	AHC	Raw	HC	AHC	P-AHC
CS	47.7	-	-	0.5	-	-	0.3	-	-	0.1	-	-	-
ES	15.2	-	-	0.6	-	-	24.3	-	-	0.1	-	-	-
DM	44.1	55.2	55.3	2.6	2.5	2.5	2.3	2.4	10.0	0.7	0.9	1.7	2.8
1:1:0	45.9	56.5	60.6	1.6	1.9	2.4	1.3	1.4	3.4	0.4	0.4	1.0	1.3
2:1:0	45.3	56.7	63.6	1.9	2.1	3.2	1.6	1.6	4.0	0.5	0.6	1.4	1.7
1:0:1	29.7	27.8	5.9	1.6	0.6	0.0	13.3	19.4	32.1	0.4	0.4	0.7	2.4
2:0:1	34.5	35.1	13.4	1.9	1.0	0.6	9.6	14.8	25.5	0.5	0.5	0.9	3.5
1:1:1	35.7	37.6	21.6	1.2	1.0	0.8	9.0	12.8	25.1	0.3	0.3	0.6	2.9
2:1:1	39.1	42.0	25.4	0.8	1.5	1.2	6.6	9.9	22.9	0.2	0.4	0.9	3.2

Note: Due to resource limitations, the data represents one measurement per sample. Single feedstock CS and ES were not used to produce HC/AHC. Hence, the table does not have values for those parameters (-).

The carbon content in AHC decreased from 63.6% to 5.9% with the increase in eggshell ratio in the mixes, whereas the calcium content increased from 3.4% to 32.1%, which could be due to the decomposition of $CaCO_3$ in eggshell to CaO and CO_2 at higher temperatures [49]. This suggests that Ca in the eggshell was successfully coated on AHC. Liu et al. (2019) reported a similar trend of decrease in carbon from 46.6% to 4.32% and increase in calcium from 1% to 42.2% with the increase in eggshell ratio in biochar prepared from rice straw. An increase in Ca content from 2.3% to 10% was also observed for AHC produced from dairy manure, which could be due to the presence of $CaCO_3$ in the animal's diet [62,66]. A previous study reported an increase in Ca content of biochar produced from dairy manure from 3.12% to 9.75% with the increase in temperature from 25 to 500 °C [62]. An increase in P content was observed after adsorption for all the adsorbents, indicating P adsorption.

3.3. Phosphate Adsorption in Batch Experiment

The hydrochar prepared from different feedstock mixes showed poor P adsorption capacities of 1–62 mg P/g (Table 4). Takaya et al. (2016) [67] reported similar results, with hydrochar produced from different wastes (such as oak wood, greenhouse waste, anaerobically digested waste, and treated municipal waste) showing poor P adsorption capacities of 0–30 mg/g. However, P adsorption improved significantly for all activated samples with eggshell, while activation did not have much impact on P adsorption of feedstock mixes without eggshell. No significant improvement was observed in the P adsorption performance of AHC prepared from dairy manure only and mixes of dairy manure and corn stover. This result indicates that the addition of corn stover did not play a significant role in the adsorption property of hydrochar.

Comparison of P adsorption capacities of AHC and AFM showed significantly high adsorption for AHC with eggshell. AHC with a DM/CS/ES ratio of 1:0:1 demonstrated a high adsorption capacity of 209 mg P/g, while AFM showed an adsorption capacity of 115 mg P/L for the same mix ratio. Previous studies have demonstrated high P adsorption performance of Ca-modified char prepared from various feedstocks, with adsorption capacities ranging from 72 to 314 mg/g (Table 5). For example, Liu et al. (2019) [13] reported that biochar produced from a 1:1 mix ratio of rice straw and eggshell performed best with maximum P adsorption of 231 mg/g, while Kong et al. (2018) [27] found that the biochar produced from the mix of $CaCO_3$ and sludge with a ratio of 1:2 had the highest P adsorption of 116.82 mg/g. The improved P adsorption property in AHC with eggshell can be due to the presence of Ca^{2+} on the surface of char and an increase in pore size and surface area during activation due to the release of CO_2 during calcination of $CaCO_3$ [13,20,39,49].

Liu et al. (2019) [13] reported an increase in pore size of the adsorbent from 6.40 to 13.1 nm when eggshell was mixed with rice straw in the ratio of 1:1.

Table 4. P adsorption of adsorbents prepared from different feedstock mixes with and without HTC and activation.

Feedstock Mix DM/CS/ES	q_e (mg/g)		
	HC	AHC	AFM
1:0:0	7.84 ± 3.99 ^{e}	7.93 ± 0.542 ^{e}	5.44 ± 1.64 ^{e}
1:1:0	1.09 ± 1.09 ^{e}	8.32 ± 1.11 ^{e}	8.13 ± 4.39 ^{e}
2:1:0	10.00 ± 2.54 ^{e}	7.11 ± 0.57 ^{e}	6.67 ± 0.77 ^{e}
1:0:1	62.20 ± 10.20 ^{d}	209.00 ± 0.60 ^{a}	115.00 ± 3.76 ^{c}
2:0:1	1.96 ± 0.75 ^{e}	198.00 ± 1.67 ^{a}	153.00 ± 0.62 ^{b}
1:1:1	10.90 ± 2.74 ^{e}	200.00 ± 1.77 ^{a}	171.00 ± 4.12 ^{b}
2:1:1	0.87 ± 0.58 ^{e}	157.00 ± 3.19 ^{b}	122.00 ± 4.22 ^{c}

Note: HC: hydrochar; AHC: activated hydrochar; and AFM: activated feedstock mix. Values are means ± standard error of means. a–e: Means in a row without a common superscript letter differ ($p < 0.05$) as analyzed by two-way ANOVA and the LSD test.

Table 5. Comparison of phosphate adsorption capacities (q_{max}) of various adsorbents in different studies.

Types of Adsorbents	P Adsorption Capacity q_{max} (mg/g)	References
Dairy manure and eggshell-activated hydrochar	209.0	This study
Eggshell-modified peanut shell biochar	191.1	[18]
Eggshell and palm fiber biochar	72.0	[68]
Eggshell-modified biochar	136.8	[39]
Sewage sludge and eggshell biochar	107.0	[69]
Rapeseed and eggshell biochar	109.7	[22]
Ca-modified biochar	129.8	[70]
Rice straw and eggshell biochar	231.0	[13]
Ca-decorated biochar	116.8	[27]
Ca-modified biochar	314.2	[43]

3.3.1. Adsorption Isotherm Model

The P adsorption amount for AHC with eggshell increased with the increase in initial concentration of P from 0 to 500 mg/L, with equilibrium adsorption being achieved at approximately 200 mg/L (Figure 2). However, AHC without eggshell had low adsorption capacity; hence, an increase in concentration did not show much impact on the adsorption performance. A previous study conducted by Wang et al. (2018) [43] for Ca-modified biochars prepared from $Ca(OH)_2$ and flour showed an increase in P adsorption from 100 to 300 mg/L, with equilibrium adsorption attained at 300 mg/L.

The Langmuir and Freundlich models were used to fit the experimental data to infer the adsorption behavior (Figure 3). The experimental results indicated better fit to the Langmuir isotherm, with a higher R^2 value compared to the Freundlich isotherm (Table 6), suggesting homogeneous monolayer adsorption. Similar observations were reported by previous studies that investigated the P adsorption mechanism of various Ca-modified biochar [13,27,43]. The highest predicted model value for P adsorption capacity was 192.91 mg/g, which was exhibited by the mix with a DM/CS/ES ratio of 1:0:1 (Table 6).

3.3.2. Adsorption Kinetic Model

The rate of P adsorption onto various AHC mixes was investigated using kinetic studies. The adsorption of P was rapid during the initial 2.5 h and slowed down, achieving equilibrium at around 6 h (Figure 4). A similar result was reported by Wang et al. (2018) [43], where the P adsorption rate of Ca-modified char increased rapidly within 1.5 h and equilibrium was attained at 2 h.

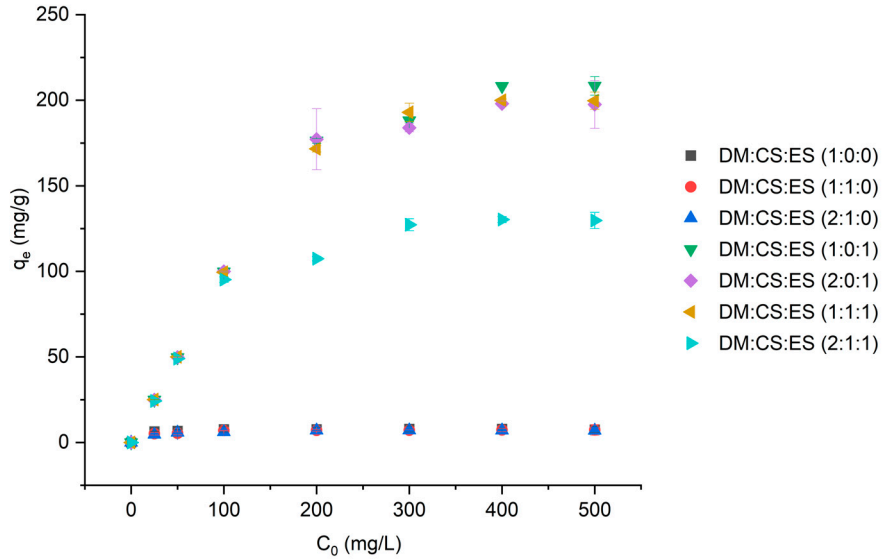

Figure 2. Amount of P adsorbed at different initial concentrations (adsorbent dose: 1 g/L, initial concentrations: 25–500 mg/L). Values are means ± standard error of means. C_0 is initial concentration, and q_e is equilibrium concentration.

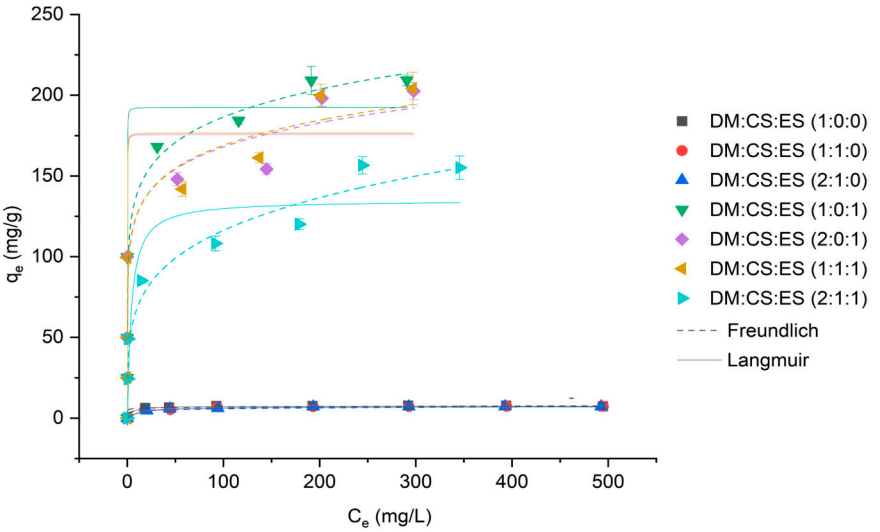

Figure 3. Langmuir and Freundlich model fit for the adsorption isotherm experiment (adsorbent dose: 1 g/L, initial concentration: 25–500 mg/L). Values are means ± standard error of means. C_e is the initial concentration, and q_e is the equilibrium concentration.

Table 6. Fitting P adsorption isotherm for various adsorbents.

Feedstock Mix DM/CS/ES	Langmuir Model			Freundlich Model		
	K_L	q_{max} (mg/g)	R^2	K_F	1/n	R^2
1:0:0	0.22	7.87	0.9947	5.65	0.056	0.7732
1:1:0	0.10	7.44	0.9854	3.77	0.112	0.8337
2:1:0	0.08	7.41	0.9955	3.46	0.126	0.9171
1:0:1	39.13	192.91	0.9341	104.44	0.126	0.9173
2:0:1	40.78	176.06	0.8974	95.87	0.122	0.8760
1:1:1	36.45	176.96	0.8802	94.77	0.126	0.8780
2:1:1	0.25	135.30	0.8925	40.58	0.230	0.9516

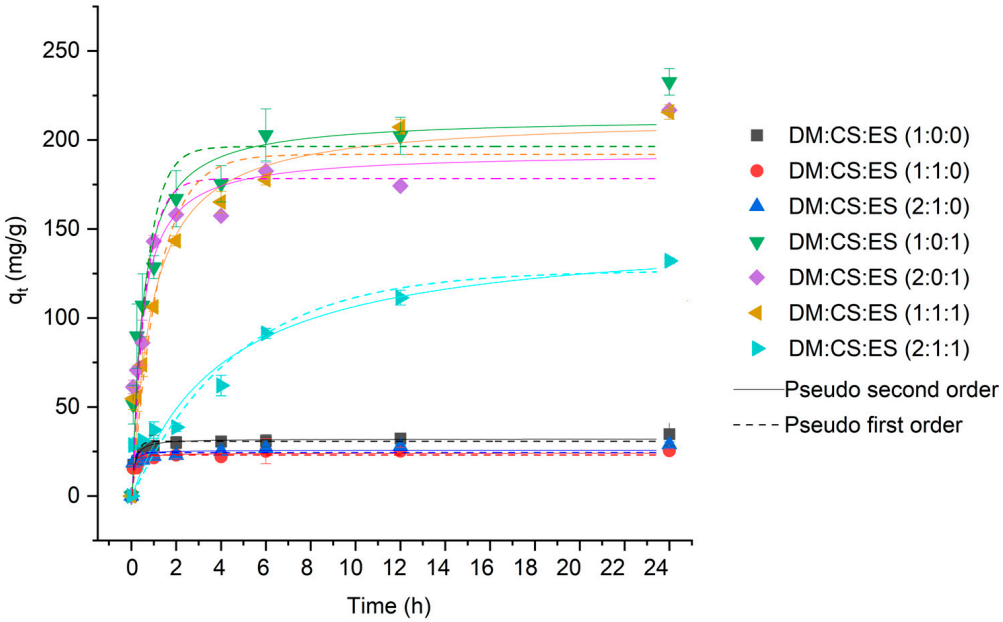

Figure 4. Adsorption kinetics of phosphate on various activated hydrochar (dose—0.01 mg, initial phosphate concentration—100 mg/L). Values are means ± standard error of means. q_t is concentration at time 't'.

Pseudo-first-order and pseudo-second-order kinetic model fitting results are shown in Table 7. The higher coefficient of determination (R^2) for pseudo-second-order confirmed that it explains the kinetics of P adsorption better. Previous studies have reported better fit to the pseudo-second-order kinetic model when using Ca-modified biochar prepared from corn stalk [20], rice straw and eggshell [13], and flour [43]. This result indicates chemisorption is the dominant mechanism for P adsorption involving chemical reactions between P and Ca [13,20,43].

Table 7. Adsorption kinetic parameters of phosphate on activated hydrochar.

Feedstock Mix DM/CS/ES	Pseudo-First-Order Model			Pseudo-Second-Order Model		
	k_1 (/h)	q_e (mg/g)	R^2	k_2 (/h)	q_e (mg/g)	R^2
1:0:0	5.856	30.681	0.9130	0.314	32.041	0.9669
1:1:0	9.535	22.919	0.8886	0.617	24.009	0.9517
2:1:0	16.143	24.312	0.8654	0.798	25.580	0.9225
1:0:1	1.491	197.317	0.9103	0.010	213.878	0.9636
2:0:1	1.632	179.255	0.9026	0.012	193.878	0.9383
1:1:1	0.832	192.916	0.9213	0.005	214.223	0.9612
2:1:1	0.208	127.272	0.8818	0.002	150.564	0.8989

3.4. Characterization of Adsorbent Before and After Adsorption

3.4.1. SEM Analysis

The SEM images of hydrochar and activated hydrochar before and after P adsorption for different feedstock mixes are shown in Figure 5. Hydrochar samples for most of the feedstock mixes before activation showed less pore formation (Figure 5(1a–4a)). Hydrochar prepared from dairy manure (Figure 5(1a)) had a smooth surface, whereas the irregular surface was observed for hydrochar prepared from mixes of dairy manure and corn stover, which could be due to the removal of hemicellulose from the cell wall during HTC [65,71]. Hydrochar with eggshell in the feedstock mixes (Figure 5(3a,4a)) showed smaller particles attached on the surface, which could be a coating of $CaCO_3$ from eggshell [18]. The lower P adsorption capacity of the hydrochar could be explained by the lack of porous structure on its surface and incomplete calcination of $CaCO_3$ due to the low HTC temperature [49,50].

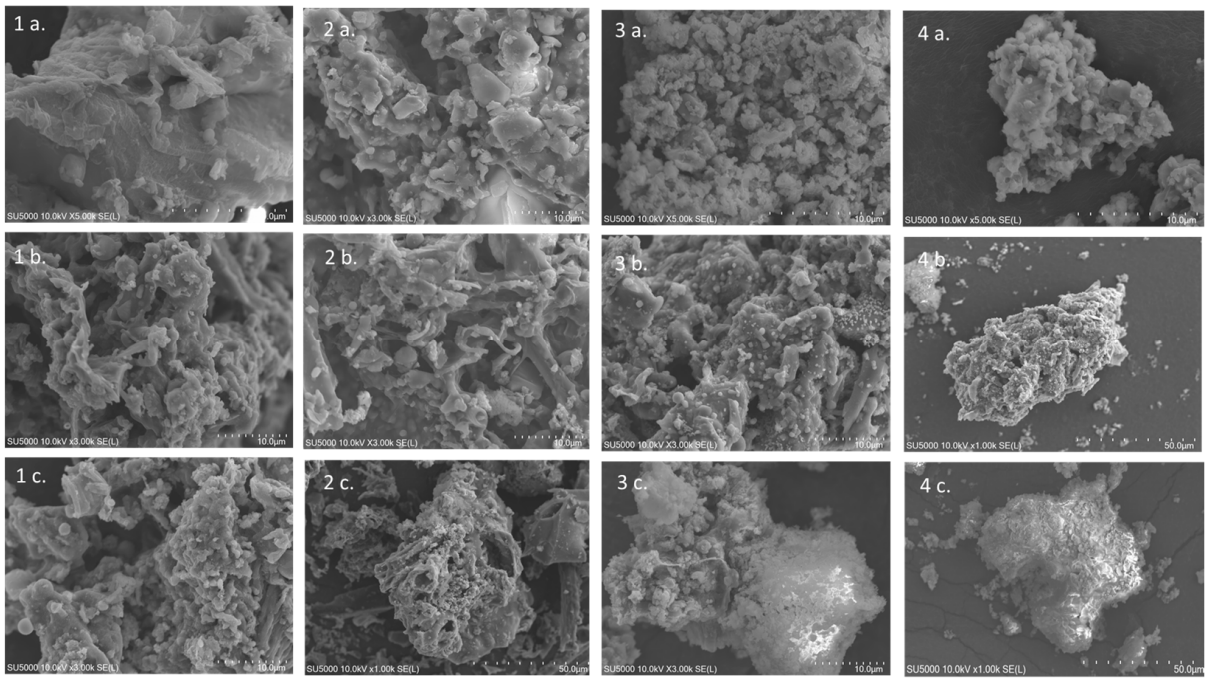

Figure 5. SEM images of hydrochar for different feedstock mixes (DM/CS/ES ratios of (1) 1:0:0, (2) 1:1:0, (3) 1:0:1, and (4) 1:1:1) and experimental steps ((**a**) before activation, (**b**) after activation, and (**c**) after P adsorption). Note: Different feedstock mix ratios of DM/CS/ES were selected to observe the morphology of the control (1:0:0) and the impact of the addition of corn stover only (1:1:0), eggshell only (1:0:1), and both corn stover and eggshell (1:1:1).

Structural changes with the development of pores were observed after activation (Figure 5(1b–4b)). Activation at higher temperatures causes degradation of organic compounds and gasification of volatile compounds, causing the formation of pores and an increase in the surface area of the char [34,62]. In addition, AHC with eggshell (Figure 5(3b,4b)) had granules attached to the surface, which could be CaO produced during the calcination process. The decomposition of $CaCO_3$ at higher temperatures above 600 °C releases CO_2, which acts as an activation agent and broadens the pore size to increase the specific surface area and pore volume of the char (Figure 5(3b,4b)) [13,26,39,49].

When comparing the morphological changes of the adsorbent before and after P adsorption, no changes were observed for hydrochar produced from mixes without eggshell (Figure 5(1b,1c,2b,2c)), which can be explained by the low P adsorption performance in the batch experiment. However, for the AHC with eggshell, clusters of the flocculent precipitate were seen adhering to the adsorbent after P adsorption (Figure 5(3c,4c)). Previous studies have reported similar results, where the surface of CaO-modified biochar produced from rice straw [13] and eggshell-modified biochar prepared from peanut shell [18] were covered with white precipitates after P adsorption due to the generation of Ca-P precipitates. The adsorption mechanism can be explained by the following chemical equations [43]:

$$3PO_4^{3-} + 5Ca^{2+} + OH^- \rightarrow Ca_5(PO_4)_3(OH) \downarrow \quad (7)$$

$$3HPO_4^{2-} + 5Ca^{2+} + 4OH^- \rightarrow Ca_5(PO_4)_3(OH) \downarrow + 3H_2O \quad (8)$$

$$3H_2PO_4^- + 5Ca^{2+} + 7OH^- \rightarrow Ca_5(PO_4)_3(OH) \downarrow + 6H_2O \quad (9)$$

3.4.2. FTIR Analysis

The AHC prepared from the sample mix with a DM/CS/ES ratio of 1:0:1 performed best, with the highest P adsorption capacity. Therefore, the sample mix was selected for FTIR analysis. The samples before and after adsorption were analyzed to identify the

functional groups and understand the interaction and bonding formed between them. As shown in Figure 6, bending vibration at 871 cm^{-1}, assigned to the C-O group, was observed both before and after adsorption, which indicates the group did not contribute to P adsorption [18,43]. A distinct change in the adsorption band at 1024 cm^{-1}, assigned to P-O, was observed after adsorption, confirming adsorption of P onto AHC [43]. An increase in P content for AHC after adsorption further confirmed P adsorption by AHC (Table 3). Similarly, a band was observed at 1421 cm^{-1} before and after adsorption, suggesting C=C did not contribute to P adsorption [18]. Wang et al. (2018) [43] reported the occurrence of bending vibration at 3573 cm^{-1} for AHC before adsorption, which was assigned to the -OH bond. The disappearance of the -OH group after P adsorption suggested favorable interaction between P and -OH loaded from $Ca(OH)_2$. Due to noise in the wavelength above 3000 cm^{-1}, it was hard to detect the -OH function group in the sample before adsorption. According to previous studies, Ca-PO_4 precipitation is the primary mechanism responsible for phosphate adsorption [27,40,43].

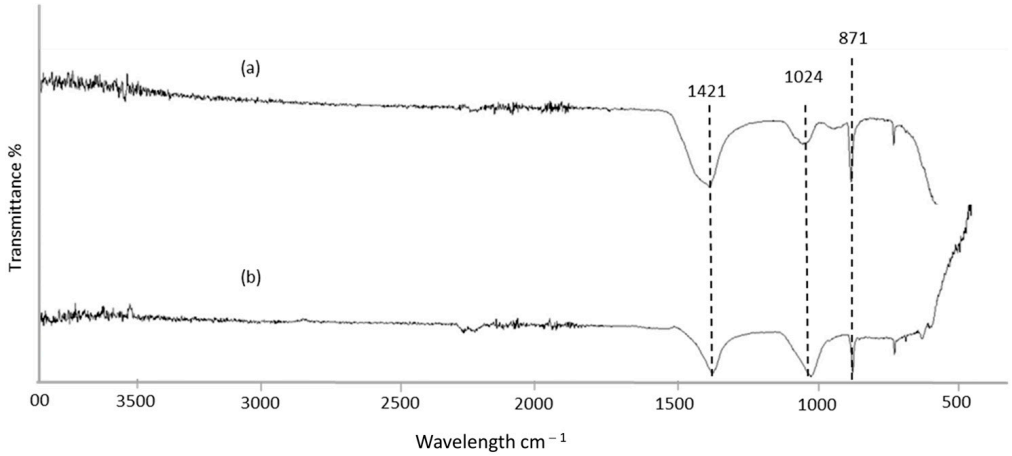

Figure 6. FTIR spectra of activated hydrochar (DM/CS/ES ratio of 1:0:1) (**a**) before P adsorption (**b**) after P adsorption. Note: Only the AHC with the highest P adsorption was used for FTIR analysis.

3.5. Phosphate Adsorption in Column Experiment

3.5.1. Effect of Adsorbent Dose on Breakthrough Curve

The result showed that breakthrough time and exhaust time increased with the increase in adsorbent dose from 0.5 to 1 g for both the concentrations in all the tested adsorbents (Figure 7). AHC prepared from feedstock mix with a DM/CS/ES ratio of 1:0:1 performed best, with the longest time to reach break point and exhaust point. With the increase in adsorbent dose from 0.5 to 1 g, breakthrough and exhaust times increased from 150 to 210 min and 450 to 540 min, respectively, at a constant inlet P concentration of 25 mg/L. AHC prepared from feedstock mixes with DM/CS/ES ratios of 2:0:1, 1:1:1, and 2:1:1 reached breakthrough and exhaust times more quickly compared to a DM/CS/ES ratio of 1:0:1. However, an increase in breakthrough and exhaust time were observed with the increase in adsorbent dose. Similar trends were reported in previous studies for P [26,72] and other pollutants, such as heavy metals [73] and pharmaceutical compounds [74]. For example, Yan et al. (2014) [26] reported an increase in breakthrough time from 130 to 330 min and exhaust time from 310 to 700 min for an increase in adsorbent bed height from 15 to 25 cm at an initial P concentration of 50 mg/L. Similarly, an increase in breakthrough time from 190 to 348 min was reported with an increase in bed height from 5 to 8 cm at a constant inlet concentration of 10 mg/L [56]. This delay in breakthrough and exhaust time with the increase in adsorbent dose could be attributed to more available adsorption sites and longer residence time within the column, allowing better P adsorption [56,75]. This indicated that the column saturated faster at a lower adsorbent dose, while a higher dose required a longer time to exhaust.

3.5.2. Effect of Initial Phosphate Concentration on Breakthrough Curve

The result showed that the break point and exhaust point were attained more quickly when the inlet concentration was increased from 25 to 50 mg/L for all the samples (Figure 8). AHC prepared from feedstock mix with a DM/CS/ES ratio of 1:0:1 had the longest breakthrough and exhaust times of 210 and 540 min, respectively, at an initial concentration of 25 mg/L and an adsorbent dose of 1 g. As the influent concentration increased from 25 to 50 mg/L, the breakthrough and exhaustion times decreased from 210 to 150 min and 540 to 450 min, respectively. A previous study reported a decrease in exhaust time from 1000 to 420 min with the increase in concentration from 20 to 100 mg/L [26], while another study found a decrease in exhaust time from 381 to 292 min with the increase in concentration from 10 to 25 mg/L [56]. The lower P concentration caused slower diffusion of P onto the adsorbent surface, while the higher concentration resulted in a higher concentration gradient and lower mass resistance, leading to shorter breakthrough and exhaustion times [56]. Similar results were reported when using aluminum-loaded biochar [59] and electrochemically modified calcium alginate beads [57] to remove P from an aqueous solution. The results indicated faster saturation of the column at higher initial concentrations.

3.5.3. Thomas Model Fit with the Experimental Values

The Thomas model was used to predict the fixed-bed column parameters in continuous flow. The coefficient of determination (R^2) values were between 0.9710 and 0.9985, indicating a strong fit between the experimental and model-predicted values (Table 8). In most of the runs, the values of k_{th} and q_0 decreased with the increase in adsorbent dose. The decrease in q_0 could be due to the increase in channeling effect with the increase in dose, reducing the column capacity [53,76]. A similar trend was reported by other studies on P removal using different adsorbents [26,53,56,58,76]. However, k_{th} decreased and q_0 increased with an increase in initial concentration. This could be due to the increase in driving force at higher concentrations. These results are similar to the findings from previous studies [26,53,56,58,77].

Table 8. Parameters obtained from the non-linear Thomas model for P adsorption in a fixed-bed column.

Feedstock Mix DM/CS/ES	C_0 (mg/L)	Adsorbent Dose (g)	Experimental Values	Thomas Model		
			q_e (mg/g)	K_{th} (mL/min mg)	q_0 (mg/g)	R^2
1:0:1	50	1.0	60.15 ± 1.68	0.67	60.67	0.9962
	25	1.0	45.21 ± 4.27	0.71	45.34	0.9952
	50	0.5	65.97 ± 9.04	0.65	62.03	0.9826
	25	0.5	64.30 ± 9.60	0.82	62.49	0.9808
2:0:1	50	1.0	26.64 ± 2.63	0.97	25.41	0.9840
	25	1.0	20.80 ± 0.91	0.93	21.40	0.9806
	50	0.5	26.36 ± 5.02	1.63	29.05	0.9980
	25	0.5	23.10 ± 1.75	2.28	21.93	0.9985
1:1:1	50	1.0	23.31 ± 0.19	1.03	22.92	0.9980
	25	1.0	19.59 ± 0.65	1.13	19.04	0.9870
	50	0.5	38.40 ± 0.98	1.26	31.92	0.9710
	25	0.5	24.00 ± 1.64	2.03	23.50	0.9971
2:1:1	50	1.0	28.64 ± 2.22	0.99	28.38	0.9966
	25	1.0	22.93 ± 0.17	1.07	22.73	0.9905
	50	0.5	35.01 ± 1.40	1.47	34.03	0.9926
	25	0.5	28.90 ± 2.36	1.76	28.33	0.9926

Note: For experimental values (q_e), data are reported as mean ± standard error of means.

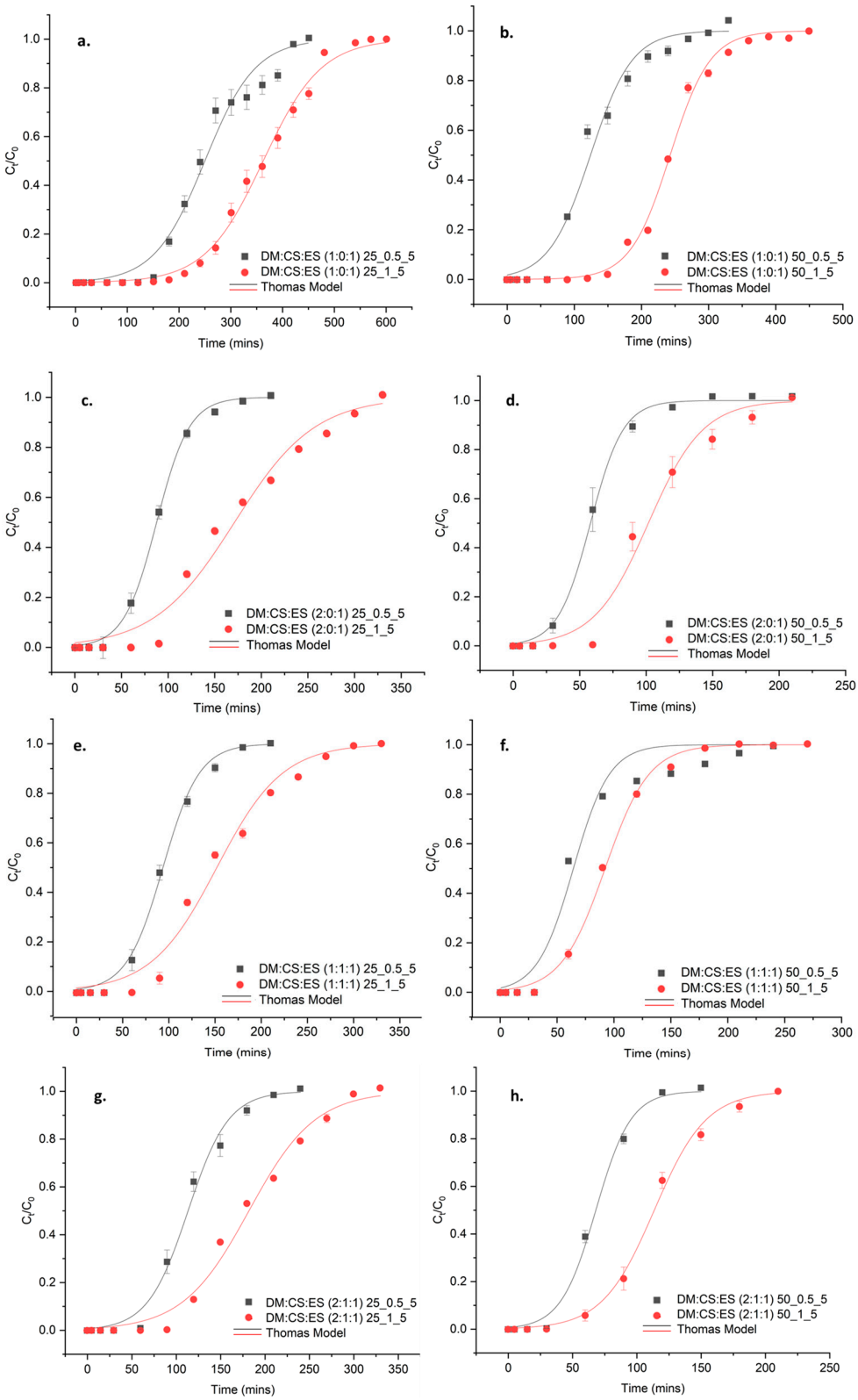

Figure 7. Effect of adsorbent dose (0.5 and 1 g) on breakthrough curve for various adsorbents: (**a**,**c**,**e**,**g**) initial concentration of 25 mg/L and flow rate of 5 mL/min; (**b**,**d**,**f**,**h**) initial concentration of 50 mg/L and flow rate of 5 mL/min (values are means ± standard error of means).

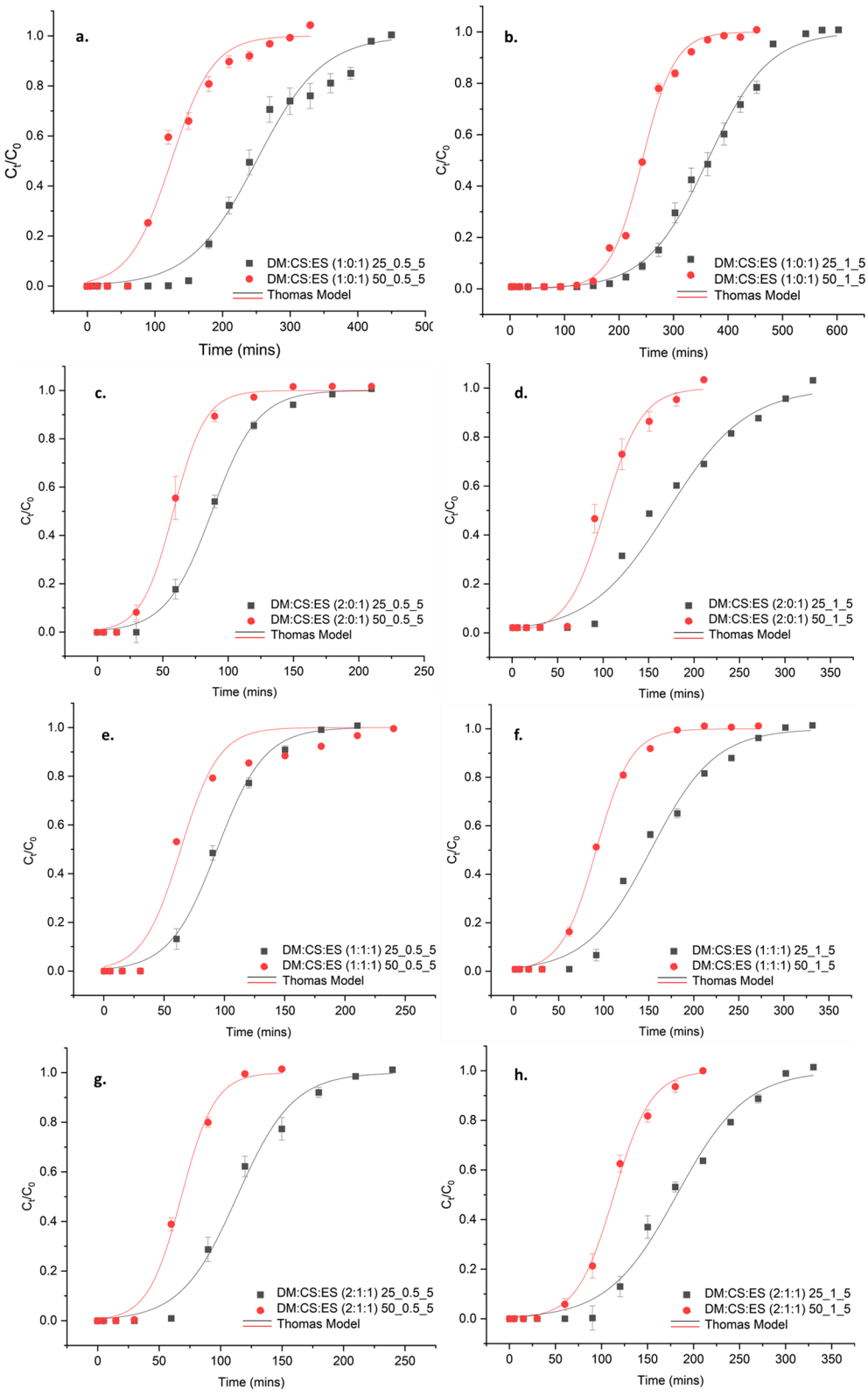

Figure 8. Effect of initial concentration (25 and 50 mg/L) on breakthrough curve shown by various adsorbents: (**a**,**c**,**e**,**g**) adsorbent dose of 0.5 g and flow rate of 5 mL/min; (**b**,**d**,**f**,**h**) adsorbent dose of 1 g and flow rate of 5 mL/min (values are means ± standard error of means).

3.5.4. Statistical Analysis

A three-way ANOVA was conducted for 16 column runs with three replications to examine the interaction effect of four feedstock mixes, two initial concentrations, and two adsorbent doses on P adsorption. As shown in Table 9, the interaction effect among three factors on P adsorption was non-significant, with a *p*-value of 0.3870. Similarly, the interaction between two factors, i.e., feedstock mix and initial concentration, feedstock mix and adsorbent dose, and initial concentration and adsorbent dose, was also non-significant, with *p*-values of 0.9734, 0.1809, and 0.9046, respectively. However, the main effect for the individual parameter—feedstock mixes, initial concentration, and adsorbent dose—was significant with *p*-values of <0.0001, 0.0035, and <0.0142, respectively, indicating they are all significant predictors of P adsorption. The AHC prepared with the feedstock mix with DM/CS/ES in a ratio of 1:0:1 showed a significantly high P adsorption capacity of 58.9 mg/g compared to the other three mix ratios (Table 10).

Table 9. ANOVA results using P adsorption as response variable.

Effect	Num DF	F Value	*p*-Value
Feedstock mix	3	45.21	<0.0001
Initial concentration	1	9.96	0.0035
Adsorbent dose	1	6.73	<0.0142
Feedstock mix × initial concentration	3	0.07	0.9734
Feedstock mix × adsorbent dose	3	1.73	0.1809
Initial concentration × adsorbent dose	1	0.01	0.9046
Feedstock mix × initial conc. × adsorbent dose	3	1.04	0.3870

The AHC prepared with the feedstock mix DM/CS/ES in a ratio of 1:0:1 showed a significantly high P adsorption capacity of 58.9 mg/g as compared to the other three mix ratios (Table 10). Similarly, the lower adsorbent dose of 0.5 g demonstrated significantly high adsorption capacity, which could be due to channeling and incomplete utilization of the column bed at a higher dose [53,74,76]. The high adsorption capacity exhibited at higher initial concentrations could be due to a higher driving force at higher initial concentrations [26,53,56].

Table 10. Impact of individual parameters (adsorbent dose, initial concentration, and feedstock mix ratios) on P adsorption.

Factors	Levels	P Adsorption (mg/g)
Adsorbent dose (g)	0.5	37.4 ± 4.1^{Aa}
	1.0	30.9 ± 2.9^{Bb}
Initial concentration (mg/L)	25	30.2 ± 3.5^{B}
	50	38.1 ± 3.5^{A}
Mix ratio (DM/CS/ES)	1:0:1	58.9 ± 4.4^{a}
	2:0:1	22.4 ± 2.3^{b}
	1:1:1	26.3 ± 2.2^{b}
	2:1:1	28.9 ± 1.6^{b}

Note: Values are means ± standard error of means. Significant differences are only compared for different levels within each factor. Means in a row without a common superscript letter are significantly different ($p < 0.05$) as analyzed by one-way ANOVA and the LSD test.

4. Conclusions

This study investigated the performance of hydrochar prepared from different feedstock mixes of dairy manure, corn stover, and eggshell via hydrothermal carbonization and thermal activation. Hydrochar exhibited poor P adsorption for all mixes. However, P adsorption improved significantly after activation for hydrochar containing eggshell, suggesting that while the addition of eggshell can improve P adsorption capacity, activation is necessary for enhanced performance. The activated hydrochar prepared with DM/CS/ES ratios of 1:0:1, 2:0:1, and 1:1:1 exhibited significantly higher P adsorption than other mixes.

The lack of a significant difference in P adsorption among the three feedstock mixes indicates that the addition of corn stover did not impact P adsorption. The Langmuir isotherm model and pseudo-second-order kinetic model showed better fit, indicating monolayer chemisorption as the mechanism of P adsorption. All the tested adsorbents effectively removed P from the solution under various adsorbent doses and inlet concentrations in the fixed-bed column. The column performed better at higher adsorbent doses and lower inlet concentrations. The Thomas model fitted well with the experimental data, indicating it can be used to predict P adsorption behavior in a fixed-bed continuous column. This study indicates that activated hydrochar with eggshell has potential in removing P from water. The promising adsorbents can be applied in nutrient removal systems to capture P from agricultural runoff, reducing nutrient load in nearby water bodies. However, this study used a chemical P solution to simulate P-rich water in agricultural runoff. Therefore, to draw further conclusions, the performance of the adsorbent can be tested under real environmental conditions using actual agricultural runoff water of varying temperatures and pH conditions. Additionally, technoeconomic analysis and life cycle assessment can provide insights into its economic feasibility and environmental impacts. This approach not only supports sustainable P removal but also addresses agricultural waste management. Moreover, P-rich hydrochar after adsorption can potentially be used as fertilizer to substitute mined P, promoting a circular economy.

Supplementary Materials: The following supporting information can be downloaded at https://www.mdpi.com/article/10.3390/su16219259/s1, Figure S1: Column apparatus set-up; Figure S2: Breakthrough curve; Table S1: Column study experimental design; Table S2: Physical properties of feedstocks and their mixes.

Author Contributions: All authors contributed to the conceptualization and design of the study. Investigation and methodology were performed by E.S. and A.M. Software and formal analysis were performed by E.S. Supervision was provided by A.M. and A.S. The first draft of the manuscript was written by E.S. Review was conducted by A.M. and A.S. All authors have read and agreed to the published version of the manuscript.

Funding: This research was funded by the Ohio State University CFAES Research and Graduate Education Internal Grants Program (award number PJ 2022-020) and United States Department of Agriculture (USDA) National Institute of Food and Agriculture (NIFA) (award number 2023-67019-39731).

Institutional Review Board Statement: Not applicable.

Informed Consent Statement: Not applicable.

Data Availability Statement: The datasets used or analyzed during the current study are available from the corresponding author upon reasonable request.

Acknowledgments: The authors would like to thank STAR Lab (https://u.osu.edu/starlab/ (accessed on 7 August 2024)) for helping with ICP analysis, MCIC OSU Wooster Campus (https://mcic.osu.edu/ (accessed on 7 August 2024)) for helping with SEM analysis, and Quasar Energy, Wooster, for providing technical support for C and N analysis.

Conflicts of Interest: The authors declare no conflicts of interest.

References

1. Manthiram, K.; Gribkoff, E. Fertilizer and Climate Change. Available online: https://climate.mit.edu/explainers/fertilizer-and-climate-change (accessed on 7 June 2022).
2. Consumption of Agricultural Fertilizers in the United States from 2010 to 2021, by Nutrient. Available online: https://www.statista.com/statistics/1330021/fertilizer-consumption-by-nutrient-us/ (accessed on 2 August 2024).
3. Usman, M.O.; Aturagaba, G.; Ntale, M.; Nyakairu, G.W. A Review of Adsorption Techniques for Removal of Phosphates from Wastewater. *Water Sci. Technol.* **2022**, *86*, 3113–3132. [CrossRef] [PubMed]
4. Rittmann, B.E.; Mayer, B.; Westerhoff, P.; Edwards, M. Capturing the Lost Phosphorus. *Chemosphere* **2011**, *84*, 846–853. [CrossRef] [PubMed]
5. Steffen, W.; Richardson, K.; Rockström, J.; Cornell, S.E.; Fetzer, I.; Bennett, E.M.; Biggs, R.; Carpenter, S.R.; De Vries, W.; De Wit, C.A. Planetary Boundaries: Guiding Human Development on a Changing Planet. *Science* **2015**, *347*, 1259855. [CrossRef]

6. Fink, G.; Alcamo, J.; Flörke, M.; Reder, K. Phosphorus Loadings to the World's Largest Lakes: Sources and Trends. *Glob. Biogeochem. Cycles* **2018**, *32*, 617–634. [CrossRef]
7. Badylak, S.; Phlips, E.J. Spatial and Temporal Distributions of Zooplankton in Tampa Bay, Florida, Including Observations during a HAB Event. *J. Plankton Res.* **2008**, *30*, 449–465. [CrossRef]
8. Hu, Z.; Sykes, R.; Davis, M.F.; Charles Brummer, E.; Ragauskas, A.J. Chemical Profiles of Switchgrass. *Bioresour. Technol.* **2010**, *101*, 3253–3257. [CrossRef]
9. Davis, T.W.; Bullerjahn, G.S.; Tuttle, T.; McKay, R.M.; Watson, S.B. Effects of Increasing Nitrogen and Phosphorus Concentrations on Phytoplankton Community Growth and Toxicity during Planktothrix Blooms in Sandusky Bay, Lake Erie. *Environ. Sci. Technol.* **2015**, *49*, 7197–7207. [CrossRef] [PubMed]
10. Jabbar, F.K. Statistical Assessment of Nonpoint Source Pollution in Agricultural Watersheds in the Lower Grand River Watershed, MO, USA. *Environ. Sci. Pollut. Res.* **2019**, *26*, 1487–1506. [CrossRef]
11. Eaken, J.P. Toledo Invests $1 Billion in Water Treatment Plant. Available online: http://presspublications.com/content/toledo-invests-1-billion-water-treatment-plant-0 (accessed on 2 September 2020).
12. Altamira-Algarra, B.; Puigagut, J.; Day, J.W.; Mitsch, W.J.; Vymazal, J.; Hunter, R.G.; García, J.; Liu, X.; Shen, F.; Qi, X. A Review of Technologies for Closing the P Loop in Agriculture Runoff: Contributing to the Transition towards a Circular Economy. *Ecol. Eng.* **2022**, *177*, 106571. [CrossRef]
13. Liu, X.; Feng, S.; Qi, X. Adsorption Recovery of Phosphate from Aqueous Solution by CaO-Biochar Composites Prepared from Eggshell and Rice Straw. *Sci. Total Environ.* **2019**, *666*, 694–702. [CrossRef]
14. Pratt, C.; Parsons, S.A.; Soares, A.; Martin, B.D. Biologically and Chemically Mediated Adsorption and Precipitation of Phosphorus from Wastewater. *Curr. Opin. Biotechnol.* **2012**, *23*, 890–896. [CrossRef] [PubMed]
15. Zhuo, S.N.; Dai, T.C.; Ren, H.Y.; Liu, B.F. Simultaneous Adsorption of Phosphate and Tetracycline by Calcium Modified Corn Stover Biochar: Performance and Mechanism. *Bioresour. Technol.* **2022**, *359*, 127477. [CrossRef] [PubMed]
16. Tee, G.T.; Gok, X.Y.; Yong, W.F. Adsorption of Pollutants in Wastewater via Biosorbents, Nanoparticles and Magnetic Biosorbents: A Review. *Environ. Res.* **2022**, *212*, 113248. [CrossRef]
17. Chen, S.; Zhang, J.; Zhang, C.; Yue, Q.; Li, Y.; Li, C. Equilibrium and Kinetic Studies of Methyl Orange and Methyl Violet Adsorption on Activated Carbon Derived from Phragmites Australis. *Desalination* **2010**, *252*, 149–156. [CrossRef]
18. Xu, C.; Liu, R.; Chen, L.; Wang, Q. Efficient Adsorption Removal of Phosphate from Rural Domestic Sewage by Waste Eggshell-Modified Peanut Shell Biochar Adsorbent Materials. *Materials* **2023**, *16*, 5873. [CrossRef] [PubMed]
19. Zhang, S.; Pi, M.; Su, Y.; Xu, D.; Xiong, Y.; Zhang, H. Physiochemical Properties and Pyrolysis Behavior Evaluations of Hydrochar from Co-Hydrothermal Treatment of Rice Straw and Sewage Sludge. *Biomass Bioenergy* **2020**, *140*, 105664. [CrossRef]
20. Sun, C.; Cao, H.; Huang, C.; Wang, P.; Yin, J.; Liu, H.; Tian, H.; Xu, H.; Zhu, J.; Liu, Z. Eggshell Based Biochar for Highly Efficient Adsorption and Recovery of Phosphorus from Aqueous Solution: Kinetics, Mechanism and Potential as Phosphorus Fertilizer. *Bioresour. Technol.* **2022**, *362*, 127851. [CrossRef]
21. Wang, Q.; Wu, S.; Cui, D.; Pan, S.; Xu, F.; Xu, F.; Wang, Z.; Li, G. Co-Hydrothermal Carbonization of Corn Stover and Food Waste: Characterization of Hydrochar, Synergistic Effects, and Combustion Characteristic Analysis. *J. Environ. Chem. Eng.* **2022**, *10*, 108716. [CrossRef]
22. Cao, H.; Wu, X.; Syed-Hassan, S.S.A.; Zhang, S.; Mood, S.H.; Milan, Y.J.; Garcia-Perez, M. Characteristics and Mechanisms of Phosphorous Adsorption by Rape Straw-Derived Biochar Functionalized with Calcium from Eggshell. *Bioresour. Technol.* **2020**, *318*, 124063. [CrossRef]
23. Tu, W.; Liu, Y.; Xie, Z.; Chen, M.; Ma, L.; Du, G.; Zhu, M. A Novel Activation-Hydrochar via Hydrothermal Carbonization and KOH Activation of Sewage Sludge and Coconut Shell for Biomass Wastes: Preparation, Characterization and Adsorption Properties. *J. Colloid Interface Sci.* **2021**, *593*, 390–407. [CrossRef]
24. Wang, X.; Liu, S.; Gao, C.; Feng, C.; Yang, J.; Liu, M.; Wu, L. Recovery of Ammonium and Phosphate from Wastewater by Wheat Straw-Based Amphoteric Adsorbent and Reusing as a Multifunctional Slow-Release Compound Fertilizer. *ACS Sustain. Chem. Eng.* **2016**, *4*, 2068–2079. [CrossRef]
25. Xu, X.; Gao, B.; Wang, W.; Yue, Q.; Wang, Y.; Ni, S. Adsorption of Phosphate from Aqueous Solutions onto Modified Wheat Residue: Characteristics, Kinetic and Column Studies. *Colloids Surf. B Biointerfaces* **2009**, *70*, 46–52. [CrossRef] [PubMed]
26. Yan, Y.; Sun, X.; Ma, F.; Li, J.; Shen, J.; Han, W.; Liu, X.; Wang, L. Removal of Phosphate from Etching Wastewater by Calcined Alkaline Residue: Batch and Column Studies. *J. Taiwan Inst. Chem. Eng.* **2014**, *45*, 1709–1716. [CrossRef]
27. Kong, L.; Han, M.; Shih, K.; Su, M.; Diao, Z.; Long, J.; Chen, D.; Hou, L.; Peng, Y. Nano-Rod Ca-Decorated Sludge Derived Carbon for Removal of Phosphorus. *Environ. Pollut.* **2018**, *233*, 698–705. [CrossRef]
28. Stobernack, N.; Malek, C. Hydrothermal Carbonization Combined with Thermochemical Treatment of Sewage Sludge: Effects of MgCl2 on the Migration of Phosphorus and Heavy Metal. *Waste Manag.* **2023**, *165*, 150–158. [CrossRef]
29. Peng, G.; Jiang, S.; Wang, Y.; Zhang, Q.; Cao, Y.; Sun, Y.; Zhang, W.; Wang, L. Synthesis of Mn/Al Double Oxygen Biochar from Dewatered Sludge for Enhancing Phosphate Removal. *J. Clean. Prod.* **2020**, *251*, 119725. [CrossRef]
30. Lin, J.C.; Mariuzza, D.; Volpe, M.; Fiori, L.; Ceylan, S.; Goldfarb, J.L. Integrated Thermochemical Conversion Process for Valorizing Mixed Agricultural and Dairy Waste to Nutrient-Enriched Biochars and Biofuels. *Bioresour. Technol.* **2021**, *328*, 124765. [CrossRef]
31. Fu, M.; Mo, C.; Li, H.; Zhang, Y.; Huang, W. Comparison of Physicochemical Properties of Biochars and Hydrochars Produced from Food Wastes. *J. Clean. Prod.* **2019**, *236*, 117637. [CrossRef]

32. Pagliari, P.; Wilson, M.; He, Z. Animal Manure Production and Utilization: Impact of Modern Concentrated Animal Feeding Operations. In *Animal Manure*; Wiley: Hoboken, NJ, USA, 2020; pp. 1–14.
33. Wang, D.; Chen, N.; Yu, Y.; Hu, W.; Feng, C. Investigation on the Adsorption of Phosphorus by Fe-Loaded Ceramic Adsorbent. *J. Colloid Interface Sci.* **2016**, *464*, 277–284. [CrossRef]
34. Mariuzza, D.; Lin, J.-C.; Volpe, M.; Fiori, L.; Ceylan, S.; Goldfarb, J.L. Impact of Co-Hydrothermal Carbonization of Animal and Agricultural Waste on Hydrochars' Soil Amendment and Solid Fuel Properties. *Biomass Bioenergy* **2022**, *157*, 106329. [CrossRef]
35. Koundinya, V. Corn Stover. Available online: https://www.agmrc.org/commodities-products/biomass/corn-stover (accessed on 17 April 2024).
36. Wright, L.L.; Perlack, R.D.; Turnhollow, A.F.; Eaton, L.M. Switchgrass Production in the USA. Available online: https://www.ieabioenergy.com/wp-content/uploads/2018/01/IEA_Bioenergy_Task43_PR2011-03.pdf (accessed on 8 August 2024).
37. Chen, Z.-L.; Zhang, J.-Q.; Huang, L.; Yuan, Z.-H.; Li, Z.-J.; Liu, M.-C. Removal of Cd and Pb with Biochar Made from Dairy Manure at Low Temperature. *J. Integr. Agric.* **2019**, *18*, 201–210. [CrossRef]
38. Li, H.Z.; Zhang, Y.N.; Guo, J.Z.; Lv, J.Q.; Huan, W.W.; Li, B. Preparation of Hydrochar with High Adsorption Performance for Methylene Blue by Co-Hydrothermal Carbonization of Polyvinyl Chloride and Bamboo. *Bioresour. Technol.* **2021**, *337*, 125442. [CrossRef] [PubMed]
39. Wang, L.; Wang, J.; Wei, Y. Facile Synthesis of Eggshell Biochar Beads for Superior Aqueous Phosphate Adsorption with Potential Urine P-Recovery. *Colloids Surfaces A Physicochem. Eng. Asp.* **2021**, *622*, 126589. [CrossRef]
40. Jiang, D.; Chu, B.; Amano, Y.; Machida, M. Removal and Recovery of Phosphate from Water by Mg-Laden Biochar: Batch and Column Studies. *Colloids Surfaces A Physicochem. Eng. Asp.* **2018**, *558*, 429–437. [CrossRef]
41. Shin, H.; Tiwari, D.; Kim, D.J. Phosphate adsorption/desorption kinetics and P bioavailability of Mg-biochar from ground coffee waste. *J. Water Process Eng.* **2020**, *37*, 101484. [CrossRef]
42. Li, R.; Wang, J.J.; Zhou, B.; Awasthi, M.K.; Ali, A.; Zhang, Z.; Lahori, A.H.; Mahar, A. Recovery of Phosphate from Aqueous Solution by Magnesium Oxide Decorated Magnetic Biochar and Its Potential as Phosphate-Based Fertilizer Substitute. *Bioresour. Technol.* **2016**, *215*, 209–214. [CrossRef] [PubMed]
43. Wang, S.; Kong, L.; Long, J.; Su, M.; Diao, Z.; Chang, X.; Chen, D.; Song, G.; Shih, K. Adsorption of Phosphorus by Calcium-Flour Biochar: Isotherm, Kinetic and Transformation Studies. *Chemosphere* **2018**, *195*, 666–672. [CrossRef]
44. Liu, Q.; Xu, R.; Yan, C.; Han, L.; Lei, H.; Ruan, R.; Zhang, X. Fast Hydrothermal Co-Liquefaction of Corn Stover and Cow Manure for Biocrude and Hydrochar Production. *Bioresour. Technol.* **2021**, *340*, 125630. [CrossRef]
45. Qin, X.; Meng, W.; Cheng, S.; Xing, B.; Shi, C.; Nie, Y.; Wang, Q.; Xia, H. Efficient Removal of Heavy Metal and Antibiotics from Wastewater by Phosphate-Modified Hydrochar. *Chemosphere* **2023**, *345*, 140484. [CrossRef]
46. Tran, T.H.; Le, A.H.; Pham, T.H.; Nguyen, D.T.; Chang, S.W.; Chung, W.J.; Nguyen, D.D. Adsorption Isotherms and Kinetic Modeling of Methylene Blue Dye onto a Carbonaceous Hydrochar Adsorbent Derived from Coffee Husk Waste. *Sci. Total Environ.* **2020**, *725*, 138325. [CrossRef]
47. Hames, B.; Ruiz, R.; Scarlata, C.; Sluiter, A.; Sluiter, J.; Templeton, D. *Preparation of Samples for Compositional Analysis*; NREL: Golden, CO, USA, 2008.
48. Sluiter, A.; Hames, B.; Ruiz, R.; Scarlata, C.; Sluiter, J.; Templeton, D. *Determination of Ash in Biomass*; NREL: Golden, CO, USA, 2008.
49. Köse, T.E.; Kivanç, B. Adsorption of Phosphate from Aqueous Solutions Using Calcined Waste Eggshell. *Chem. Eng. J.* **2011**, *178*, 34–39. [CrossRef]
50. Panagiotou, E.; Kafa, N.; Koutsokeras, L.; Kouis, P.; Nikolaou, P.; Constantinides, G.; Vyrides, I. Turning Calcined Waste Egg Shells and Wastewater to Brushite: Phosphorus Adsorption from Aqua Media and Anaerobic Sludge Leach Water. *J. Clean. Prod.* **2018**, *178*, 419–428. [CrossRef]
51. U.S. Environmental Protection Agency. Method 365.3: Phosphorous, All Forms (Colorimetric, Ascorbic Acid, Two Reagent). 1978. Available online: https://www.epa.gov/sites/default/files/2015-08/documents/method_365-3_1978.pdf (accessed on 7 August 2024).
52. Wang, J.; Guo, X. Adsorption Isotherm Models: Classification, Physical Meaning, Application and Solving Method. *Chemosphere* **2020**, *258*, 127279. [CrossRef] [PubMed]
53. Ramirez, A.; Giraldo, S.; García-Nunez, J.; Flórez, E.; Acelas, N. Phosphate Removal from Water Using a Hybrid Material in a Fixed-Bed Column. *J. Water Process Eng.* **2018**, *26*, 131–137. [CrossRef]
54. Zhang, Y.P.; Adi, V.S.K.; Huang, H.L.; Lin, H.P.; Huang, Z.H. Adsorption of Metal Ions with Biochars Derived from Biomass Wastes in a Fixed Column: Adsorption Isotherm and Process Simulation. *J. Ind. Eng. Chem.* **2019**, *76*, 240–244. [CrossRef]
55. Zhang, X.; Li, Y.; Wu, M.; Pang, Y.; Hao, Z.; Hu, M.; Qiu, R.; Chen, Z. Enhanced Adsorption of Tetracycline by an Iron and Manganese Oxides Loaded Biochar: Kinetics, Mechanism and Column Adsorption. *Bioresour. Technol.* **2021**, *320*, 124264. [CrossRef]
56. Mekonnen, D.T.; Alemayehu, E.; Lennartz, B. Fixed-Bed Column Technique for the Removal of Phosphate from Water Using Leftover Coal. *Materials* **2021**, *14*, 5466. [CrossRef]
57. Jung, K.W.; Jeong, T.U.; Choi, J.W.; Ahn, K.H.; Lee, S.H. Adsorption of Phosphate from Aqueous Solution Using Electrochemically Modified Biochar Calcium-Alginate Beads: Batch and Fixed-Bed Column Performance. *Bioresour. Technol.* **2017**, *244*, 23–32. [CrossRef]

58. Jang, J.; Lee, D.S. Effective Phosphorus Removal Using Chitosan/Ca-Organically Modified Montmorillonite Beads in Batch and Fixed-Bed Column Studies. *J. Hazard. Mater.* **2019**, *375*, 9–18. [CrossRef]
59. Zheng, Y.; Wang, B.; Wester, A.E.; Chen, J.; He, F.; Chen, H.; Gao, B. Reclaiming Phosphorus from Secondary Treated Municipal Wastewater with Engineered Biochar. *Chem. Eng. J.* **2019**, *362*, 460–468. [CrossRef]
60. Bulgariu, D.; Bulgariu, L. Bioresource Technology Sorption of Pb (II) onto a Mixture of Algae Waste Biomass and Anion Exchanger Resin in a Packed-Bed Column. *Bioresour. Technol.* **2013**, *129*, 374–380. [CrossRef] [PubMed]
61. Zhang, C.; Zheng, C.; Ma, X.; Zhou, Y.; Wu, J. Co-Hydrothermal Carbonization of Sewage Sludge and Banana Stalk: Fuel Properties of Hydrochar and Environmental Risks of Heavy Metals. *J. Environ. Chem. Eng.* **2021**, *9*, 106051. [CrossRef]
62. Cao, X.; Harris, W. Bioresource Technology Properties of Dairy-Manure-Derived Biochar Pertinent to Its Potential Use in Remediation. *Bioresour. Technol.* **2010**, *101*, 5222–5228. [CrossRef] [PubMed]
63. Yue, Y.; Lin, Q.; Xu, Y.; Li, G.; Zhao, X. Slow Pyrolysis as a Measure for Rapidly Treating Cow Manure and the Biochar Characteristics. *J. Anal. Appl. Pyrolysis* **2017**, *124*, 355–361. [CrossRef]
64. Wu, K.; Gao, Y.; Zhu, G.; Zhu, J.; Yuan, Q.; Chen, Y.; Cai, M.; Feng, L. Characterization of Dairy Manure Hydrochar and Aqueous Phase Products Generated by Hydrothermal Carbonization at Different Temperatures. *J. Anal. Appl. Pyrolysis* **2017**, *127*, 335–342. [CrossRef]
65. Liu, Z.; Zhang, Y.; Liu, Z. Comparative Production of Biochars from Corn Stalk and Cow Manure. *Bioresour. Technol.* **2019**, *291*, 121855. [CrossRef]
66. Manure Value. 2024. Available online: https://water.unl.edu/manure-value (accessed on 4 February 2024).
67. Takaya, C.A.; Fletcher, L.A.; Singh, S.; Anyikude, K.U.; Ross, A.B. Phosphate and Ammonium Sorption Capacity of Biochar and Hydrochar from Different Wastes. *Chemosphere* **2016**, *145*, 518–527. [CrossRef]
68. Pérez, S.; Muñoz-Sadaña, J.; Acelas, N.; Flórez, E. Phosphate Removal from Aqueous Solutions by Heat Treatment of Eggshell and Palm Fiber. *J. Environ. Chem. Eng.* **2021**, *9*, 104684. [CrossRef]
69. Yang, J.; Zhang, M.; Wang, H.; Xue, J.; Lv, Q.; Pang, G. Efficient Recovery of Phosphate from Aqueous Solution Using Biochar Derived from Co-Pyrolysis of Sewage Sludge with Eggshell. *J. Environ. Chem. Eng.* **2021**, *9*, 105354. [CrossRef]
70. Fang, L.; Li, J.-S.; Donatello, S.; Cheeseman, C.; Poon, C.S.; Tsang, D.C. Use of Mg/Ca Modified Biochars to Take up Phosphorus from Acid-Extract of Incinerated Sewage Sludge Ash (ISSA) for Fertilizer Application. *J. Clean. Prod.* **2020**, *244*, 118853. [CrossRef]
71. Lin, Q.-X.; Zhang, C.-H.; Wang, X.-H.; Cheng, B.-G.; Mai, N.; Ren, J.-L. Impact of Activation on Properties of Carbon-Based Solid Acid Catalysts for the Hydrothermal Conversion of Xylose and Hemicelluloses. *Catal. Today* **2019**, *319*, 31–40. [CrossRef]
72. Jurado-Davila, V.; De Oliveira, J.T.; Estumano, D.; Féris, L.A. Fixed-Bed Column for Phosphate Adsorption Combining Experimental Observation, Mathematical Simulation, and Statistics: Classical and Bayesian. *Sep. Purif. Technol.* **2023**, *317*, 123914. [CrossRef]
73. Patel, H. Batch and Continuous Fixed Bed Adsorption of Heavy Metals Removal Using Activated Charcoal from Neem (Azadirachta Indica) Leaf Powder. *Sci. Rep.* **2020**, *10*, 16895. [CrossRef] [PubMed]
74. de Franco, M.A.E.; de Carvalho, C.B.; Bonetto, M.M.; de Pelegrini Soares, R.; Féris, L.A. Diclofenac Removal from Water by Adsorption Using Activated Carbon in Batch Mode and Fixed-Bed Column: Isotherms, Thermodynamic Study and Breakthrough Curves Modeling. *J. Clean. Prod.* **2018**, *181*, 145–154. [CrossRef]
75. Jung, J.; Maeda, M.; Chang, A.; Bhandari, M.; Ashapure, A.; Landivar-Bowles, J. The Potential of Remote Sensing and Artificial Intelligence as Tools to Improve the Resilience of Agriculture Production Systems. *Curr. Opin. Biotechnol.* **2021**, *70*, 15–22. [CrossRef]
76. Paudyal, H.; Pangeni, B.; Inoue, K.; Kawakita, H.; Ohto, K.; Alam, S. Adsorptive Removal of Fluoride from Aqueous Medium Using a Fixed Bed Column Packed with Zr (IV) Loaded Dried Orange Juice Residue. *Bioresour. Technol.* **2013**, *146*, 713–720. [CrossRef]
77. Abid, M.; Altufaily, M.; Al-mansori, N.J. Mathematical Modeling of Fixed-Bed Columns for the Adsorption of Methylene Blue on to Fired Clay Pot. *Int. J. ChemTech Res.* **2019**, *12*, 70–80.